Ray/Beam Tracing for Modeling the Effects of Ocean and Platform Dynamics

John C. Peterson and Michael B. Porter, *Senior Member, IEEE*

***Abstract*—In recent years, there have been notable technical advances in modulation schemes for underwater acoustic communications, and inexpensive commercial modems are now readily available. This has generated a renewed interest in modeling the effects of the underwater sound channel on the transmission of a known time series. The previously developed Virtual Timeseries Experiment (VirTEX) algorithm addressed the need for such models. It utilizes a sequence of ray-tracing computations on temporal snapshots of the environment. This approach can handle practical environments with arbitrary source, receiver, or sea-surface motion. While VirTEX can model the transmission of a known time series to any desired accuracy, its utility is offset by the computational resources required. In this paper, we present two new algorithms for modeling the propagation of a known time series in a restricted class of time-varying environments. The first algorithm can address steady motion of the source and/or receiver. The second algorithm can address a moving sea surface that satisfies some simple constraints. While more restrictive and less accurate than VirTEX, these new algorithms are significantly faster and more efficient. This makes them much more attractive for applications involving the modeling of extensive "what-if" scenarios. The algorithms can be implemented in software by postprocessing of the output from popular ray-tracing computer programs.**

***Index Terms*—Hardware in loop, ray tracing, time-varying environments, underwater communications.**

I. Introduction

MODELING the effects of the underwater sound channel on the transmission of a known time series has historically been based on ray-tracing methods [1]–[5]. By design, ray-tracing methods compute the impulse response or time arrival structure of the sound channel for a given source and receiver location. The time series observed at a hypothetical receiver can be modeled by convolving the transmitted time series with the time arrival structure of the sound channel. The utility of this approach is limited by the fact that currently available ray-tracing algorithms are designed for environments where the source, receiver, and media boundaries are assumed to be stationary.

Manuscript received November 20, 2012; revised May 01, 2013; accepted August 12, 2013. Date of publication September 13, 2013; date of current version October 09, 2013. This work was supported by the U.S. Office of Naval Research, Code OA322, under contract N00014-12-C 0359.

Associate Editor: J. Potter; Guest Editor: J. Preisig.

The authors are with Heat, Light and Sound Research, Inc., La Jolla, CA 92037-1025 USA (e-mail: jcp@hlsresearch.com).

Color versions of one or more of the figures in this paper are available online at http://ieeexplore.ieee.org.

Digital Object Identifier 10.1109/JOE.2013.2278914

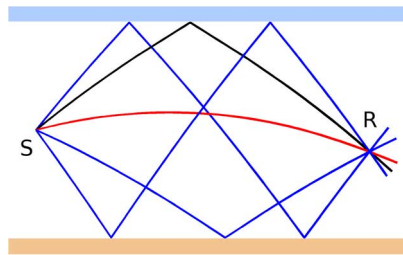

Fig. 1. Notional ray-trace calculation showing the eigenrays; all of the possible acoustic paths from the source (denoted by $\mathbf{S}$), to the receiver (denoted by $\mathbf{R}$).

Most environments of practical interest involve some form of motion; the moving air–sea interface, as well as source and receiver motion are common examples. This paper will present two new algorithms for modeling the effects of the sound channel on the transmission of a known time series. The algorithms support a restricted, but useful class of environmental motion. They require more modest computational resources than existing algorithms, and can easily be implemented in software by postprocessing of the output from popular ray-tracing computer programs.

The structure of this paper is as follows. Section II will present the necessary extensions to the background mathematics of ray tracing for modeling time-varying environments. Section III will present a summary of the Virtual Timeseries Experiment (VirTEX) algorithm [6], as well as our two new algorithms. Section IV will present some practical applications of the new algorithms to the evaluation of underwater acoustic modem performance in time-varying environments.

II. Modeling Time-Varying Environments Using Ray-Tracing Methods

As noted above, the modeling of the effects of the underwater sound channel on the transmission of a known time series has historically been approached using ray-tracing methods. The central computation is the integration of the ray approximation to the acoustic wave equation with respect to time. The eigenrays which represent the paths through the sound channel from the source to a receiver can be identified by tracing a suitably dense "fan" of rays emanating from the source. Those rays that pass through the given receiver are classified as eigenrays, as shown in Fig. 1.

Existing ray-tracing algorithms provide a complex valued amplitude A_i and an elapsed or travel time τ_i that quantify what is observed at the given receiver for each eigenray $i = 1 \ldots N$. The amplitudes A_i are complex valued to reflect phase changes associated with any interactions with the sea bottom or due to caustics. The time series observed at the receiver, denoted by

$r(t)$, is given by the convolution of the source time series, denoted by $s(t)$, with the impulse response of the sound channel. This is the sum over the N eigenrays given by

$$r(t) = \sum_{i=1}^{N} \mathrm{Re}\{A_i\} s(t-\tau_i) - \mathrm{Im}\{A_i\} \mathcal{S}(t-\tau_i) \qquad (1)$$

where $\mathcal{S}(t)$ denotes the Hilbert transform of the source time series $s(t)$. We will show how this approach can be readily extended to address the additional issues associated with time-varying environments in the following section.

A. Extending Ray-Tracing Methods to Time-Varying Environments

To model propagation in time-varying environments, the constant valued travel times used for static environments are generalized to become functions of the source, receiver position, and transmission time [7], [8]. To this end, we denote the arrival function associated with a given eigenray as

$$\tau\left(t, \vec{\mathbf{x}}_s(t), \vec{\mathbf{x}}_r(t+\tau)\right). \qquad (2)$$

It represents the elapsed or travel time of a disturbance transmitted by the source at time t and position $\vec{\mathbf{x}}_s(t)$, and arriving at the receiver at time $t+\tau$ and position $\vec{\mathbf{x}}_r(t+\tau)$. Note that τ is implicitly defined whenever the receiver is moving.

A rigorous algorithm for computing the arrival function can be constructed from suitable extensions to existing ray-tracing methods designed for static environments. These extensions address the issues related to environmental motion *during* the integration of the ray equations with respect to time. (For example, the precise determination of the time when an eigenray intersects a *moving* media boundary is more complicated. The distance from the eigenray to the closest point on the moving boundary must vanish at the intersection event.) This approach would produce a *time-dependent* ray tracer. It computes the value of the arrival function corresponding to a single value of the independent variable t. In general, the entire process must be repeated for a different value of t.

This approach is not conceptually difficult, and contemporary computers are powerful enough to make this approach feasible. However, we will show in Section III that, for certain types of environmental motion, an acceptable approximation to the arrival function can be computed with much less effort.

III. Approximations to the Arrivals Function

A. A Brief Review of the VirTEX Algorithm

One of the primary advantages of the VirTEX algorithm [6] is that it can model most forms of environmental motion. The time-varying environment of interest is approximated by a temporal sequence of *static environments* that span the time interval of interest, each one representing a "snapshot" in time of the moving environment. A ray-tracing computation is performed for each of the static environments, producing a set of eigenrays with complex amplitudes and arrival times that describe the propagation through the sound channel at the instant associated with that snapshot.

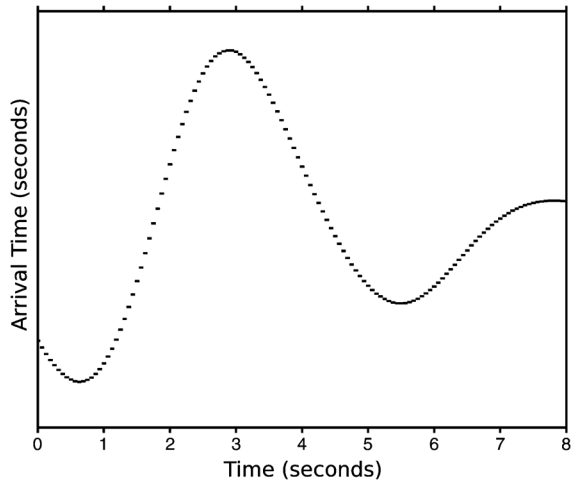

Fig. 2. A notional example of the piecewise continuous approximation to the arrival function for a single eigenray as computed by the VirTEX algorithm.

It should be noted that VirTEX is *not* a time-dependent ray tracer. In the real world, the environment (e.g., sea surface) is moving during the time that the eigenray transits the sound channel. The transit time can be long enough for significant motion to occur (particularly in deep-water environments). However, in each "snapshot" ray-tracing calculation in the VirTEX algorithm, the environment is assumed to be *static* during the entire time that the rays transit the sound channel. Therefore, the causality of surface bounce events for eigenrays that interact with the sea surface are not modeled exactly.

Putting aside the details of the implementation of the VirTEX algorithm, the end result is that the arrival function takes the form of a piecewise continuous function such as the notional example shown in Fig. 2. The error introduced by using a piecewise continuous representation of the arrival function can be reduced to any desired level by reducing the time difference between the temporal snapshots of the environment (at the expense of the resources required to perform the additional ray-tracing calculations).

While the VirTEX algorithm is capable of modeling arbitrary time-varying environments, certain forms of environmental motion can be readily modeled with much less computational effort and without significantly compromising accuracy. The case of a source and/or receiver that is moving with constant velocity is one such example that is commonly encountered and is addressed in Section III-B.

B. The Case of Steady Source and/or Receiver Motion

Without loss of generality, consider the case of a source that is fixed, a receiver moving with constant velocity, and the rest of the environment is assumed to be stationary. Let θ denote the angle between the receiver velocity vector $\vec{\mathbf{v}}$ and the unit vector $\hat{\mathbf{t}}$ tangent to the eigenray when it arrives at the receiver. The arrival function can be approximated by

$$\tau\left(t, \vec{\mathbf{x}}_s(t), \vec{\mathbf{x}}_r(t+\tau)\right) \approx \tau_0 + (t-t_0)\frac{|\vec{\mathbf{v}}|}{c}\cos(\theta) \qquad (3)$$

where τ_0 denotes the elapsed or travel time to the receiver for a disturbance emitted by the source at time t_0 (where τ_0 can

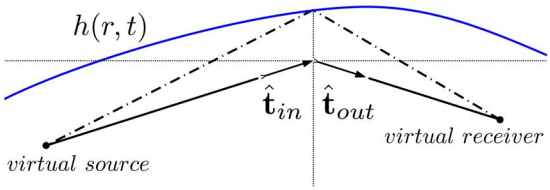

Fig. 3. Graphical depiction of the correction to the arrival time function due to sea-surface motion. The correction is the travel time associated with the dashed line (corresponding to the path that bounces off the moving sea surface) minus the travel time associated with the solid line. The solid line is obtained by extending the unit tangent vectors to the incoming and outgoing rays, obtained from the baseline ray-tracing calculation. The distances to the virtual source and receiver are *not* to scale.

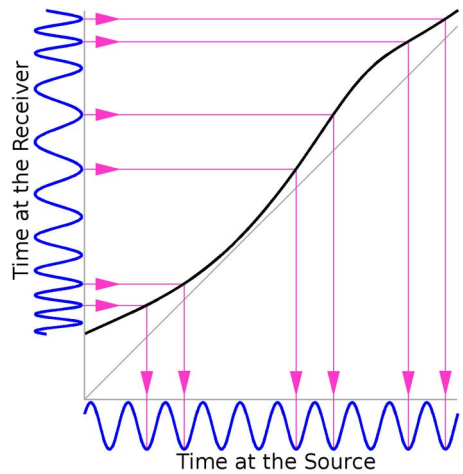

Fig. 4. A notional example of the wall clock time arrival function $w(t)$. The horizontal axis is the time t observed at the source corresponding to transmitted information. The vertical axis corresponds to the time observed when the corresponding information arrives at the receiver and is given by $w(t)$. The directed lines graphically depict the process of evaluating the inverse function $w^{-1}(t)$.

be computed using any popular ray-tracing program). For the special cases of $\cos(\theta) = \pm 1$, where the receiver velocity vector $\vec{\mathbf{v}}$ is parallel to the unit vector $\hat{\mathbf{t}}$ tangent to the eigenray at the receiver, (3) happens to be exact. For the more general case of $\cos(\theta) \neq \pm 1$, it is a very good approximation when the speed of the receiver $|\vec{\mathbf{v}}|$ is small compared to the sound speed c. This is true for the majority of situations of practical interest.

From (3), it can be shown that if the known time series transmitted by the source is given by $s(t)$, the time series observed at the receiver is given by

$$r(t) = s\left(t_0 + \frac{t - t_0 - \tau_0}{1 + \dfrac{|\vec{\mathbf{v}}|}{c}\cos(\theta)}\right). \tag{4}$$

The time series observed at a hypothetical moving receiver can be computed from a knowledge of the receiver speed $|\vec{\mathbf{v}}|$, the angle θ between the receiver velocity vector $\vec{\mathbf{v}}$, and the unit vector $\hat{\mathbf{t}}$ tangent to the eigenray when it arrives at the receiver, and the elapsed or travel time τ_0. The latter two quantities are output by most existing ray-tracing programs. When the known source time series $s(t)$ is a discretely sampled waveform (e.g., captured from a hardware modem), (4) amounts to resampling at a different sample rate. This can be efficiently accomplished using the chirp Z transform as described in [9].

Our first new algorithm, herein referred to as VirTEX for platform motion, is based on this simple result. It should be noted that (4) is an established, well-known result. Its roots can be traced back to the work of Christian Doppler, first published in 1842. Its use in underwater sound channel models has also been reported in the literature, such as [10]. However, in the case of a single source and many hypothetical receivers, the utility of (4) can be significantly enhanced by organizing the computations in an efficient manner, which we now describe.

Given some prior knowledge of the anticipated values of the receiver speed $|\vec{\mathbf{v}}|$, the arrival time series $r(t)$ as given by (4) can be *precomputed* for a suitably large set of discrete values of the dimensionless quantity $(|\vec{\mathbf{v}}|/c)\cos(\theta)$ and stored in a database. For a given source and set of hypothetical receivers, a ray-tracing program is used to compute the requisite complex amplitudes A_i, travel times τ_i, and angles θ_i for the set of receivers. At each (moving) hypothetical receiver, the observed time series is a sum of amplitude scaled and time delayed arrivals, as given in (1). For each arrival that contributes to the sum, we can look up the precomputed receiver time series associated with the closest value of the quantity $(|\vec{\mathbf{v}}|/c)\cos(\theta)$ from the database, then amplitude scale, delay, and sum, as given by (1).

Some practical examples of using VirTEX for platform motion to evaluate the performance of a simple notional modem utilizing frequency-shift keying (FSK) modulation are presented in Sections IV-B and IV-C.

C. The Case of a Moving Sea Surface

A form of motion that is present in all underwater acoustic environments is the air–sea interface. In this section, we will describe our second algorithm, herein referred to as VirTEX for sea-surface dynamics. It is designed to efficiently model the effects of the moving sea surface on the transmission of a known time series through the sound channel.

While the VirTEX for sea-surface dynamics algorithm is not particularly complicated, its description is rather lengthy. To assist the reader in gaining a better understanding of its overall structure, we will describe the algorithm in an outline format. For the sake of brevity, we will drop the arguments associated with the source and receiver positions in the arrival function, and denote it by $\tau(t)$. Begin with step (0) below and at the end of each step, proceed to the next step unless instructed otherwise.

---

0) Perform a ray-tracing calculation for the given source and receiver geometry, environmental parameters, and a *flat* air–sea interface. This baseline calculation need be done only once. (This is in contrast to the original VirTEX algorithm which requires *many* ray-tracing calculations.)

1) For each eigenray in the baseline ray-tracing calculation that intersects the sea surface at least once, we will estimate the arrival function $\tau(t)$ by conceptually moving along the eigenray from the source to the receiver, constructing it in a progressive fashion. Each time the eigenray bounces off the sea surface, we will introduce perturbations to account for the motion of the sea surface, whose height is a function of position and time, and denoted by $h(r,t)$.

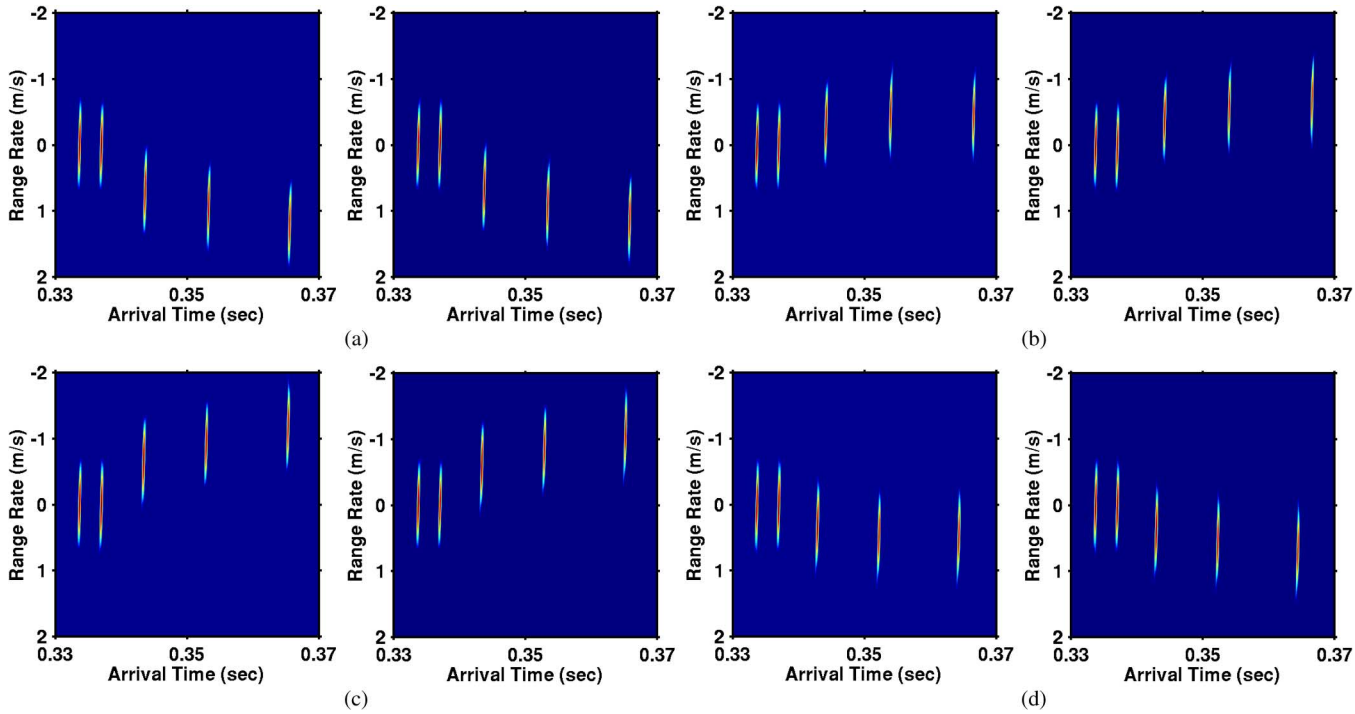

Fig. 5. The channel scattering functions for received waveforms predicted by VirTEX for sea-surface dynamics (left plots) and the original VirTEX algorithm (right plots). The moving air–sea interface is a gravity swell wave with a period of 8 s and amplitude of 2 m (or 2-m peak to trough). (a) Comparison for transmission of m-sequence at $t = 0$ s. (b) Comparison for transmission of m-sequence at $t = 2$ s. (c) Comparison for transmission of m-sequence at $t = 4$ s. (d) Comparison for transmission of m-sequence at $t = 6$ s.

The estimate will take the form of a set of tabulated values $(t_i, \tau(t_i))$ for equally spaced values of the transmit time $t_i = i\Delta t$, for $i = 0, \ldots, N$, that span the time duration of the transmitted time series. Once the estimate of the arrival function has been tabulated, it will be used to determine the specifics of the transmitted time series as observed when it arrives at the receiver along the given eigenray. For each eigenray, begin with step 1a) and perform any additional steps as indicated.

a) If this eigenray intersects the sea surface at least once or more, then proceed to the next step 1b). For eigenrays that do not interact with the sea surface, jump to step 1i).
b) Conceptually speaking, we are located at the source in this step. To reflect this, initialize all of the tabulated values of the arrival function $\tau(t_i)$ to be zero.
c) Using the baseline ray-tracing calculation performed in step 0), move along the eigenray toward the receiver to the next intersection of the eigenray with the flat sea surface. Identify the amount of time $\Delta\tau$ that has elapsed since the eigenray's *last* intersection with the sea surface (or left the source in the special case of the first interaction with the surface). Add this elapsed or travel time $\Delta\tau$ to all of the arrival function estimates $\tau(t_i)$.
d) For each of the transmit times t_i, compute the sea-surface height at the point in time when a disturbance that was transmitted by the source at time t_i arrives at the bounce point on the flat sea surface. To facilitate this calculation, we introduce the *wall clock arrival time* function, denoted by $w(t_i) = t_i + \tau(t_i)$. The choice of the term "wall clock" is to emphasize that it is analogous to reading a clock that is continuously running (as opposed to the arrival function which represents an elapsed or travel time). Using this notation, the desired sea-surface height is clearly given by $h(r, w(t_i))$, where r is provided by the baseline ray-trace calculation.
e) For each of the transmit times t_i, we will add a perturbation to the corresponding arrival function estimate $\tau(t_i)$ to account for the moving sea surface. (This step is the heart of the algorithm.) The perturbation is the difference in the travel times along two different paths, which are shown in Fig. 3.
Both paths begin at a *virtual* source and end at a *virtual* receiver (whose location will be defined shortly). The baseline path corresponds to the baseline ray-tracing calculation and consists of a straight line segment from the virtual source to the bounce point $(r, 0)$ on the flat sea surface, and a straight line segment from the bounce point to the virtual receiver. The other path represents an *estimate* of the path length of the true eigenray that bounces from the moving sea surface at the point with coordinates given by $(r, h(r, w(t_i)))$ and will now be described.
The location of the virtual source and receiver is determined from information from the baseline ray-tracing calculation. To locate the virtual source, begin by identifying the unit vector $\hat{\mathbf{t}}_{in}$ tangent to the ray *incoming* to the bounce point on the flat sea surface (this quantity is available from most ray-tracing programs). Identify the travel time $\Delta\tau$ for the eigenray from the *last* surface ounce (or when it left the source in the special case of the first bounce) to this surface bounce. Any bottom interactions that occurred during that time

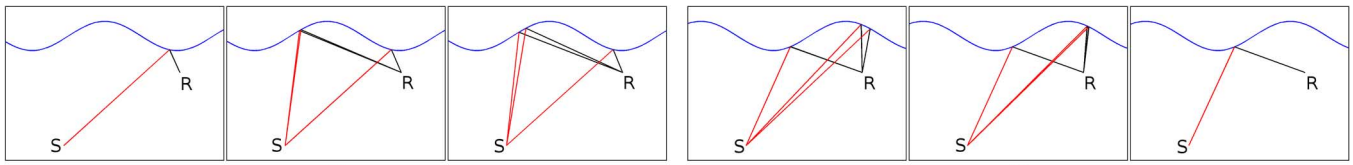

(a) (b)

Fig. 6. An example of eigenrays that appear and disappear in a Pekeris waveguide as computed by a time-dependent ray tracer. Such channel effects are *not* captured by the VirTEX for sea-surface dynamics algorithm. (a) Eigenrays appearing as time progresses (left to right). (b) Eigenrays disappearing as time progresses (left to right).

interval can be ignored by appealing to the method of images. From the bounce point, project in the direction given by $-\hat{\mathbf{t}}_{in}$ a distance equal to $\Delta\tau$ times the sound speed at the surface bounce point.
The location of the virtual receiver is computed in a similar fashion. Begin by identifying the unit vector $\hat{\mathbf{t}}_{\text{out}}$ tangent to the ray *outgoing* from the bounce point on the flat sea surface. Identify the travel time $\Delta\tau$ for the eigenray from this surface bounce to the *next* surface bounce (or when it reaches the receiver in the special case of the last bounce). From the bounce point, project in the direction given by $+\hat{\mathbf{t}}_{\text{out}}$ a distance equal to $\Delta\tau$ times the sound speed at the surface bounce point.
For each of the transmit times t_i, compute the *difference* of the length of the path that bounces from the moving sea surface at the point $(r, h(r, w(t_i)))$ and the length of the baseline path, then divide by the local sound speed at the surface bounce point. Add this perturbation to the corresponding estimate of the arrival function $\tau(t_i)$.

f) Continue along the eigenray toward the receiver. If there are any further interactions of the eigenray with the sea surface, then return to step 1c), otherwise proceed to the next step 1g).

g) From the baseline ray-tracing calculation, identify the travel time $\Delta\tau$ from the eigenray's *last* intersection with the surface to its arrival at the receiver. Add this travel time $\Delta\tau$ to all of the arrival function estimates $\tau(t_i)$.

h) At this point, we have completed the calculation of the tabulated values of the arrival function $(t_i, \tau(t_i))$ for the given eigenray. The calculation of the time series observed at the receiver from this eigenray is a straightforward process, using the tabulated values of the corresponding wall clock arrival time function $w(t_i) = t_i + \tau(t_i)$.
By definition, a disturbance that left the source at wall clock time t_s will arrive via the given eigenray at the receiver at the wall clock time $t_r = w(t_s)$. To compute the amplitude of this time series for some arbitrary time t_r at the receiver, we only need to find the time t_s such that $t_r = w(t_s)$.
The desired time t_s is given by the *inverse function* evaluated at t_r, namely, $t_s = w^{-1}(t_r)$. This can be accomplished numerically by interpolation of the tabulated vales $(w(t_i), t_i)$. A graphical depiction of the wall clock time function $w(t)$ and the process of finding t_s for a given value of t_r is shown in Fig. 4. It is not difficult to show that the inverse function $w^{-1}(t)$ exists and is unique if $w(t)$ is monotone increasing. This will be true as long as there is no (aggregate) environmental motion that exceeds the local sound speed in the media.
Once the time t_s has been determined, the desired amplitude of the time series observed at the receiver at time t_r for this eigenray is given by $\text{Re}\{A\}s(t_s) - \text{Im}\{A\}\mathcal{S}(t_s)$, where $\mathcal{S}(t)$ is the Hilbert transform of the source time series $s(t)$, and A is the complex amplitude scaling factor for this eigenray from the baseline ray-trace calculation.
We now calculate the time series observed at the receiver for this eigenray at equally spaced discrete time values. Note that the first sample of the transmit waveform is transmitted at time t_0 and arrives at the receiver at time $w(t_0)$. Similarly, the last sample of the transmit waveform is transmitted at time t_N and arrives at the receiver at time $w(t_N)$. Compute the time series observed at the receiver at the discrete times of the form $j\Delta t$, where j ranges over values so that the discrete times span the time interval $[w(t_0), w(t_N)]$. Set the computed time series aside along with the associated delay information, as the summation operation will be performed later. If there are any additional eigenrays in the baseline ray-trace calculation, return to step 1a), otherwise jump to step 2).

i) This step handles the special case of eigenrays that do *not* interact with the sea surface. In this case, the time series observed at the receiver for this eigenray can be computed as given by the terms in the summation in (1). Set the computed time series aside along with the associated delay information, as the summation will be performed later. If there are any additional eigenrays in the baseline ray-trace calculation, return to step 1a), otherwise proceed to step 2).

2) In this, the final step, we sum all of the arrival time series associated with the eigenrays taking into account their respective delays. Because of the perturbations introduced to account for interactions of the eigenrays with the sea surface, we do not know the earliest and latest arrival times until all of the above calculations are complete. While there are other ways to address this issue, a simple approach is to set aside all of the arrival time series and perform the delay and sum operation here.

The VirTEX for sea-surface dynamics algorithm is significantly faster than the original VirTEX algorithm. Most of this disparity is because the former is based on a *single* ray-tracing

TABLE I
SUMMARY OF NOTIONAL FSK MODEM DESIGN

Arrival waveform type	Standard m-sequence with configurable "chip" rate
Arrival detector type	Threshold correlator output, with CFAR threshold value
Arrival time estimator	Local search in delay space for peak correlator output
Arrival Doppler compensation	None
Data modulation scheme	Frequency Shift Keying, with "Fang" bit encoding
Data modulation parameters	Configurable symbol and reverb guard time periods
Data modulation rates	Configurable bandwidth and tone density
Data error correction scheme	None

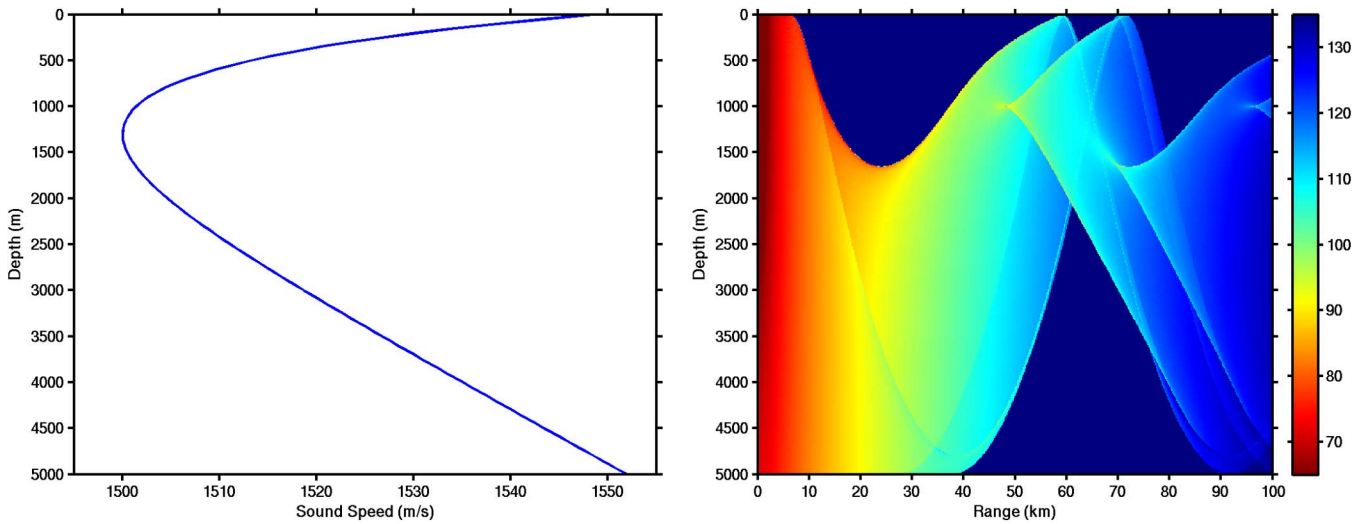

Fig. 7. Summary of idealized Munk deep-water channel environment. (a) Idealized Munk sound-speed profile. (b) Incoherent transmission loss (in decibels), source depth = 1000 m.

TABLE II
DETAILS OF SIMULATION

Description of Simulation	Fixed source and moving receivers
Sound-speed profile	Munk idealized deep water profile
Bottom depth and geoacoustic type	Absorbing bottom, 5000 m
Ambient noise spectrum level	30 dB (re: $1\mu\text{Pa}^2$ /Hz)
Source depth	1000 m
Modem center frequency	5 kHz

calculation, while the later requires *many* ray-tracing calculations (the actual number will be dependent on the rate of environmental change and the desired level of accuracy).

In the case of a single source and many hypothetical receivers, we can also take advantage of the fact that a given ray will often be an eigenray for multiple receivers. For all eigenrays, we save the results of the calculations performed in step 1d) for all the surface interactions for that ray. For any given receiver, we can retrieve the results of step 1d) for the last surface bounce before the eigenray reaches the receiver, and then continue to step 1g) to complete the calculations that are unique to the given receiver. This implementation runs at a speed roughly comparable to our implementation of VirTEX for platform motion (aside from a much longer startup time and greater memory requirements).

Our numerical experiments with VirTEX for sea-surface dynamics suggest that the algorithm delivers acceptable levels of accuracy in typical problems of practical interest. For comparison purposes, consider a Pekeris waveguide with a depth of 100 m and the air–sea interface takes the form of a gravity swell wave with a period of 8 s and amplitude of 2 m (4-m peak to trough). An m-sequence with a duration of 0.5 s is transmitted at 2-s intervals from a fixed source located at a depth of 75 m. The fixed receiver is located at 500 m in range and 50 m in depth. The predicted time series observed at the receiver were computed using VirTEX for sea-surface dynamics and the original VirTEX algorithms. The time series were then match filtered to produce the associated channel scattering functions [11]. The results of the first four transmissions are shown in Fig. 5. A comparison of the arrival functions (such as the one shown in Fig. 2) were also computed and shown to provide reasonable agreement.

While our comparisons of VirTEX for sea-surface dynamics with the original VirTEX algorithm suggest that the agreement is generally good, the new algorithm does have some limitations. The algorithm makes *no* attempt to correct the orientation of the incoming and outgoing rays at bounce points to be consistent with the orientation of the unit vector normal to the moving sea surface. (An exact treatment of this requires a time-dependent ray tracer.) These errors are small for low sea states, but become more pronounced for higher sea states.

Other, more egregious errors are possible in higher sea states because eigenrays can appear and then disappear on time scales less than the travel time from the source to the receiver. Some

examples of these artifacts are shown in Fig. 6, computed using a simple time-dependent ray-tracing algorithm for the Pekeris environment. This phenomenon is most pronounced in high sea states and for sources and receivers located close to the surface. Since our algorithm is based on a single ray-tracing calculation for a *flat* sea surface, it cannot possibly capture such effects. A more detailed discussion of the phenomenon can be found in [12].

A practical example of using VirTEX for sea-surface dynamics to evaluate the performance of a simple notional modem utilizing FSK modulation is presented in Section IV-D.

IV. Applications to Underwater Acoustic Communications

In this section, we will present some applications of the VirTEX for platform motion, and the VirTEX for sea-surface dynamics algorithms. We will utilize them to model the effects of the sound channel on the transmissions from a simple notional underwater acoustic modem. The decoding performance of an identical receiving modem as a function of position will be examined in a variety of acoustic environments, and with varying degrees of environmental motion. We have assumed that the reader has a basic understanding of the design of modern acoustic modems. A readable introduction can be found in the survey article [13].

A. FSK Modem Design

The design of the notional modem used in these examples was intentionally simplistic relative to contemporary standards. We wanted our examples to clearly convey some of the basic effects of the sound channel on the transmission of modem packets. The performance of more sophisticated modems requires a more detailed analysis to properly interpret.

The modem used in the examples to follow utilizes a maximum length sequence (m-sequence) waveform for packet detection and estimation of arrival time. The data is encoded using FSK modulation [14]. The duration of the symbol transmission and reverberation guard interval are configurable parameters. The number of tones and the bandwidth occupied by them are also configurable. Table I summarizes some of the design aspects of the modem.

It should be noted that the omission of algorithms for Doppler compensation in the packet arrival detector, and coding schemes with error correction properties was intentional. While such features are ubiquitous in contemporary modems, they obfuscate the basic effects of the sound channel that we wish to highlight.

B. Modem Performance With Moving Receivers: Deep-Water Munk Profile

In this example, the performance of the FSK modem is evaluated in a deep-water environment with a fixed source and moving receivers. The sound-speed profile is the Munk deep-water profile, with the axis of the sound channel located at a depth of 1300 m, as shown in Fig. 7(a). A perfectly absorbing bottom is located at a depth of 5000 m. The source is located slightly above the sound channel axis at a depth of 1000 m. An ambient noise level of 30 dB (re: 1 μPa^2/Hz) is simulated using additive psuedorandom Gaussian distributed noise. Table II summarizes some of the relevant parameters of the simulation.

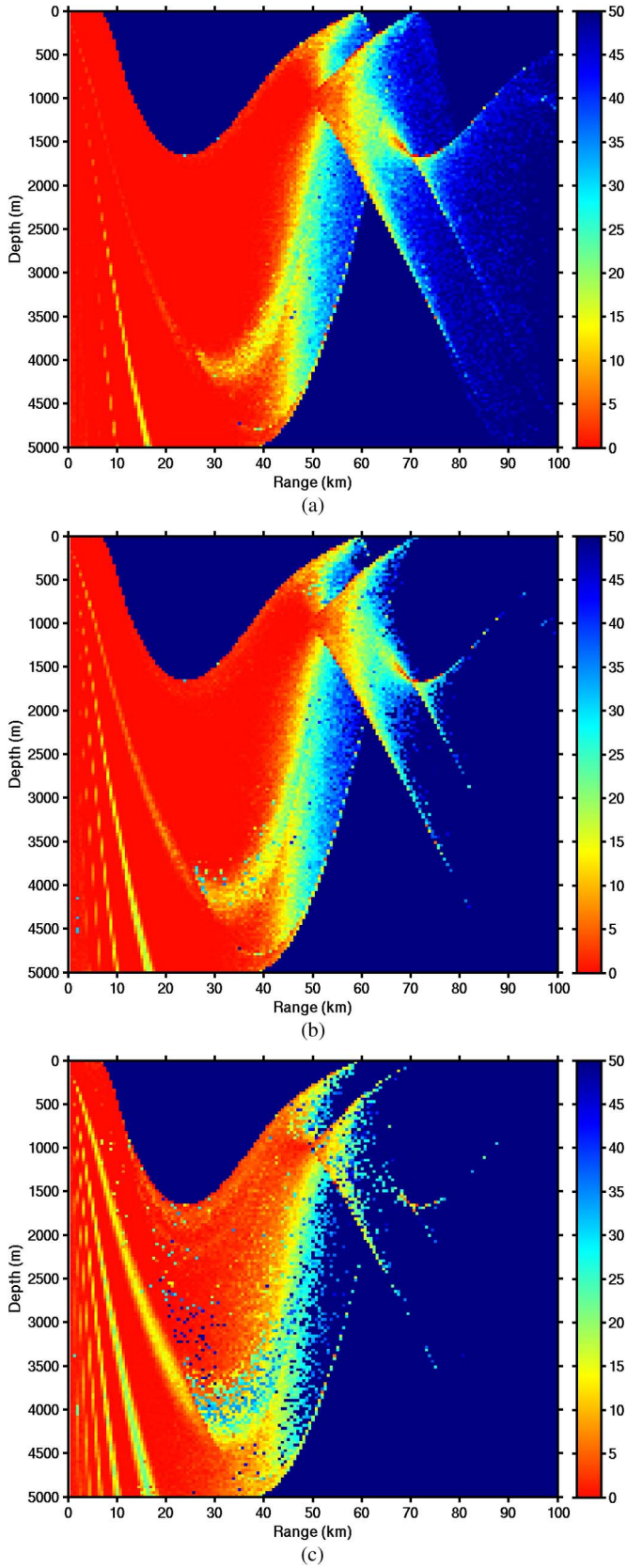

Fig. 8. Modem bit error rates (in percent), for selected values of receiver motion. (a) Case of no receiver motion. (b) Case of $|\vec{\mathbf{v}}_{rcv}| = 2.5$ m/s. (c) Case of $|\vec{\mathbf{v}}_{rcv}| = 5.0$ m/s.

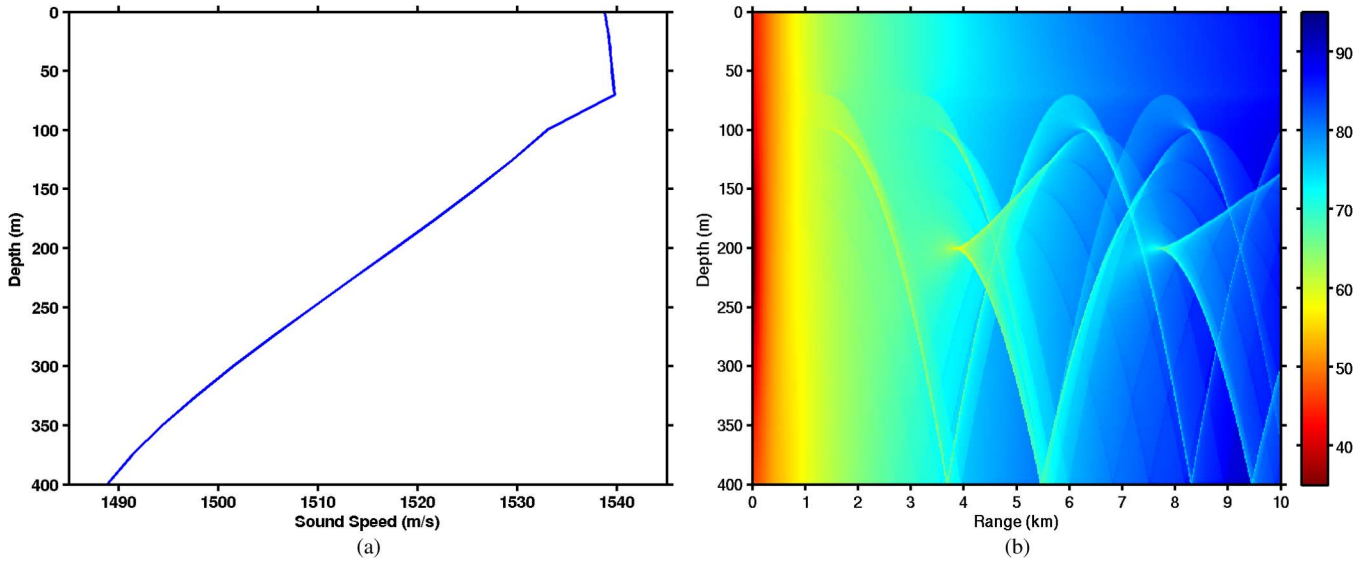

Fig. 9. Summary of downward-refracting environment. (a) Downward-refracting sound-speed profile. (b) Incoherent transmission loss (in decibels), source depth = 200 m.

TABLE III
DETAILS OF SIMULATION

Description of Simulation	Fixed source and moving receivers
Sound-speed profile	Downward refracting, with 75 m surface duct
Bottom depth and geoacoustic type	Reflective bottom, 400 m
Ambient noise spectrum level	40 dB (re: 1μPa^2 /Hz)
Source depth	200 m (below surface duct)
Modem center frequency	10 kHz

TABLE IV
DETAILS OF SIMULATION

Description of Simulation	Fixed source and receivers, moving sea-surface
Sound-speed profile	Downward refracting, with 75 m surface duct
Bottom depth and geoacoustic type	Reflective bottom, 400 m
Ambient noise spectrum level	30 dB (re: 1μPa^2 /Hz)
Source depth	65 m (in surface duct)
Modem center frequency	12 kHz

When embarking on an effort to predict acoustic modem performance, computing the transmission loss is always a good starting point. While transmission loss in itself is not necessarily a reliable predictor of performance, it is certainly true that the decoding performance of the modem will always suffer whenever the receiver is located where adequate signal energy (relative to ambient noise levels) is not present.

The incoherent transmission loss for a source placed just above the sound channel axis at a depth of 1000 m is shown in Fig. 7(b). An inspection shows that there are some deep shadow regions. Receivers in those regions see essentially no signal energy, thus there is no possibility of decoding transmissions from the source at these locations.

We now examine the impact of modem decoding performance when receiver motion is present. Fig. 8(a) shows the baseline decoding performance for the case of no receiver motion. We have intentionally extended the range of the simulation well beyond the point where the decoding performance would be considered acceptable to show the degradation of performance over a large dynamic range.

Fig. 8(b) shows the modem bit error rates (the percentage of bits that were incorrectly decoded) for the case of the receivers moving with a speed of 2.5 m/s. The receiver velocity vector $\vec{\mathbf{v}}$ is "diving" at a pitch angle of 30° from the horizontal. In this case, some degradation of decoding performance is observed in regions where it was at acceptable levels for the no motion case.

Fig. 8(c) shows the modem bit error rates for the case of the receivers moving with a speed of 5.0 m/s, and the same receiver velocity vector. In this case, additional degradation in performance is observed. Significant degradation is beginning to appear at closer ranges where performance was found to be very good for the case of no motion.

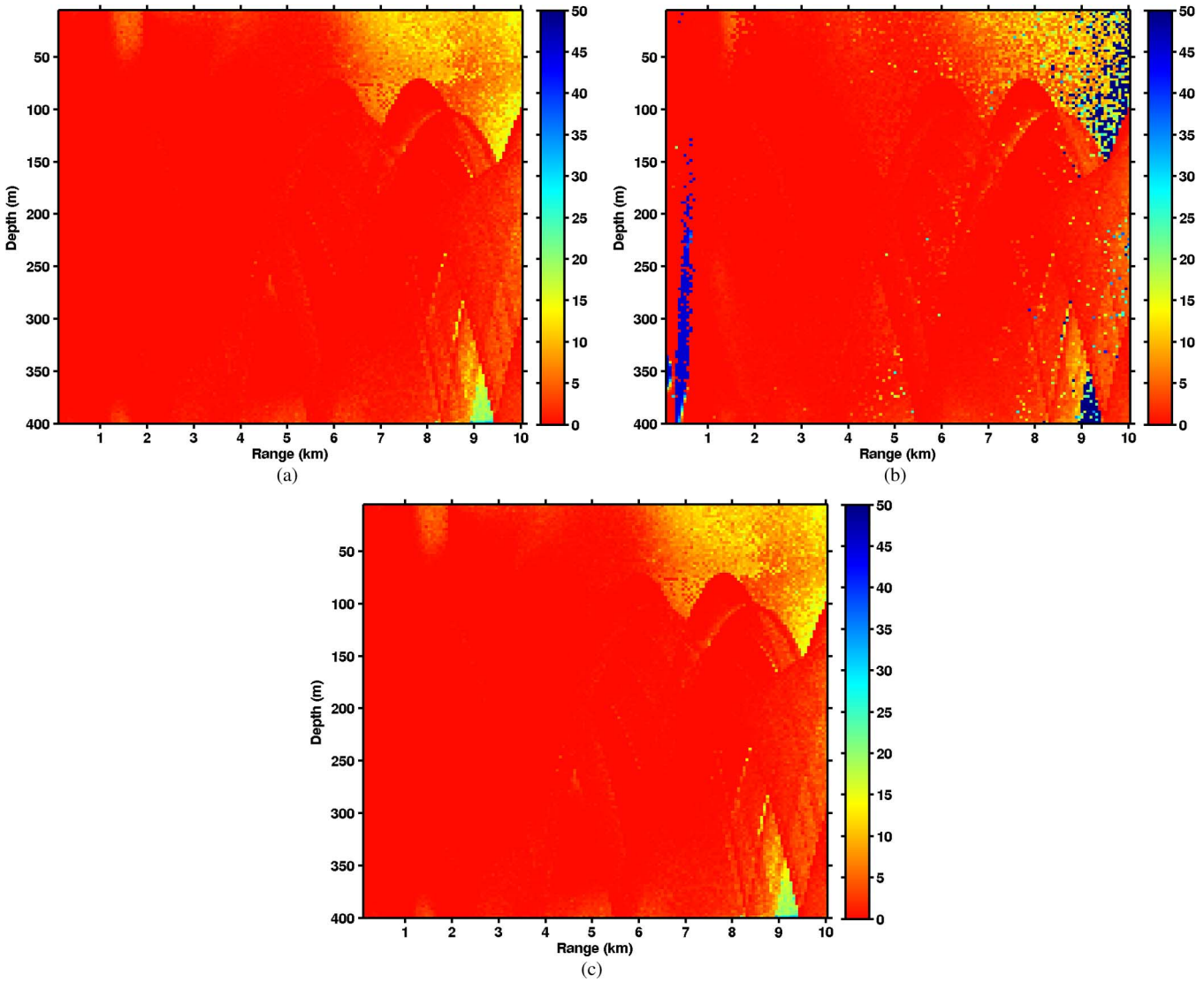

Fig. 10. Modem bit error rates (in percent), for selected values of receiver motion. (a) Case of no receiver motion. (b) Case of $|\vec{\mathbf{v}}_{rcv}| = 2.5$ m/s. (c) Case of $|\vec{\mathbf{v}}_{rcv}| = 5.0$ m/s.

C. *Modem Performance With Moving Receivers: Downward-Refracting Profile*

For this new sound-speed profile, the performance of the FSK modem is again evaluated for the case of a fixed source, and moving receivers. The sound-speed profile exhibits a surface duct down to a depth of 75 m, and a downward-refracting profile below that, as shown in Fig. 9(a). The bottom depth is 400 m, and is relatively reflective (fine sand, with a Krumbein sediment grain size of $\phi \approx 3$). The source is located below the surface duct at a depth of 200 m. Table III summarizes some of the relevant parameters of the simulation.

An inspection of the incoherent transmission loss, shown in Fig. 9(b), suggests that there should be adequate signal energy over much of the region of interest. The downward-refracting sound-speed profile combined with the reflective bottom produces eigenrays that bounce off the bottom multiple times.

The baseline decoding performance for the case of no receiver motion is shown in Fig. 10(a). As the transmission loss calculations would suggest, good decoding performance is observed over much of the region of interest.

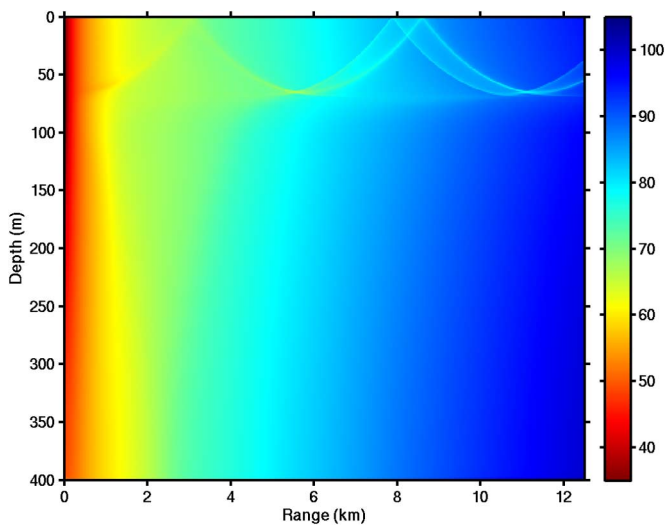

Fig. 11. Incoherent transmission loss (in decibels), source depth = 65 m.

Fig. 10(b) shows the modem bit error rates for the case of the receivers moving with a speed of 2.5 m/s. The receiver velocity

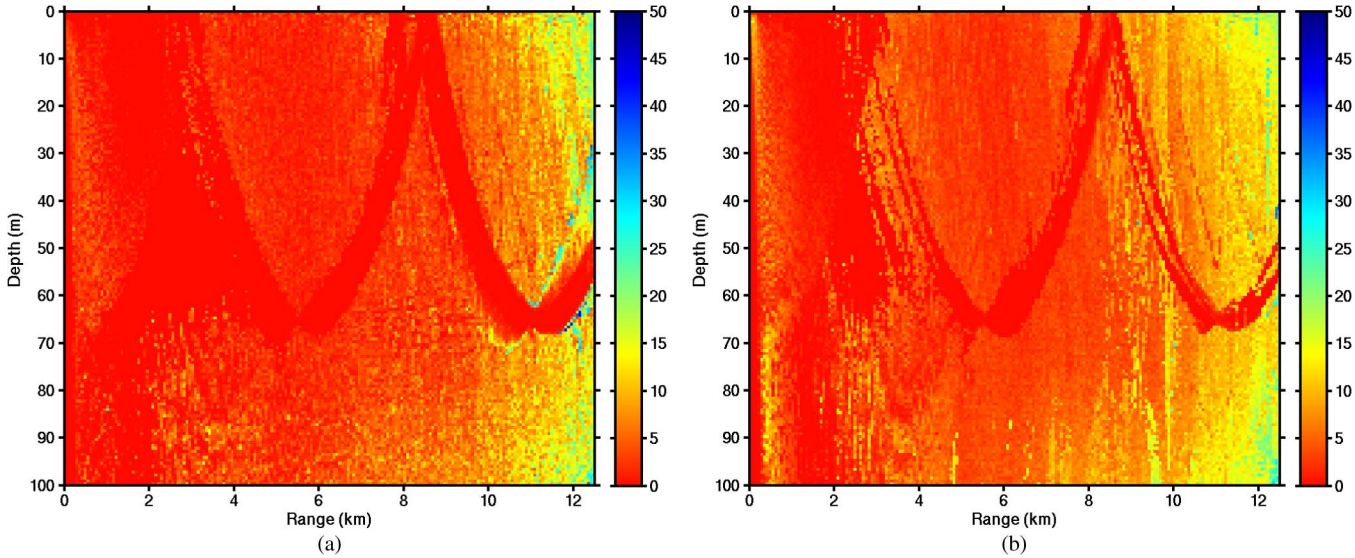

Fig. 12. Comparison of modem bit error rates (in percent), for static versus moving sea surface. (a) Case of static sea surface. (b) Case of sea state 5 (5-m peak to trough).

vector $\vec{\mathbf{v}}$ is "diving" at a pitch angle of 30° from the horizontal, as in the previous example. In this case, more serious degradation of decoding performance is observed at short ranges where it was almost perfect in the no motion case. Fig. 10(c) shows the modem bit error rates for the case of the receivers moving with a speed of 5.0 m/s. In this case, substantial degradation of decoding performance is observed over much of the region of interest.

D. Modem Performance With Moving Sea Surface: Surface Duct Profile

In our final example, the performance of the FSK modem is evaluated with the fixed source and receivers, but with a moving sea surface. The bottom depth and geoacoustic properties are identical to those in the previous example. The sound-speed profile was shown in Fig. 9(a). In this case, the source is located within the surface duct at a depth of 65 m. Table IV summarizes some of the relevant parameters of the simulation.

The incoherent transmission loss for the entire water column, calculated for the source depth of 65 m, is show in Fig. 11. For receivers located within the surface duct, adequate signal energy extends over the ranges to be simulated.

Our simple acoustic modem was designed to identify the strongest arrival within a configurable time window that follows the first detected arrival, and then compute an estimate of its arrival time. The raw symbol data associated with that arrival are then input to the decoder. In high sea states, the modem decoding performance will tend to suffer the most when the strongest arrival has interacted with the moving sea surface. Given this, we have limited our hypothetical receivers to the upper 100 m of the water column that includes the surface duct where this is often the case.

The baseline decoding performance for the case of no surface motion is shown in Fig. 12(a). Note that the decoding performance is very good within portions of the duct. Fig. 12(b) shows the modem bit error rates for a 5-m (peak to trough) swell wave. The degradation of modem performance due to sea-surface motion is often less than that observed due to platform motion of comparable magnitude. In the case of sea-surface motion, only those eigenrays that interact with the surface are altered, and modem performance may not be materially degraded unless one of those eigenrays is the dominant arrival. For the case of platform motion, all the eigenrays arriving at a receiver can potentially be altered (depending on the orientation of the eigenray relative to the receiver platform motion).

E. Evaluating the Performance of Hardware Acoustic Modems

Our new algorithms can also be used to model the performance of hardware, off-the-shelf acoustic modems. The performance of a hardware modem as a function of specific configuration settings or environmental conditions can be directly addressed by a hardware-in-the-loop simulation.

The general process begins with commanding the modem to transmit a message. The discrete sampled time series associated with the transmitted message is "captured" using a workstation equipped with suitable analog-to-digital hardware. Using either the VirTEX for platform motion or the VirTEX for sea-surface dynamics algorithm, a prediction of the time series observed at a hypothetical receiver located in the environment of interest is obtained. Using suitable digital-to-analog hardware, we then "playback" the predicted time series to the modem, and make note of the modem's decoding performance, as reported to the host computer connected to the modem.

Detailed decoding performance maps similar to those shown in the previous examples can be readily generated by sending "playback" time series associated with the hypothetical receiver positions to the modem at regular time intervals, and logging the diagnostic messages sent by the modem to the host computer in a file. The performance map can then be constructed by suitable postprocessing of the log file. The utility of this process will be heavily dependent on the availability of suitable diagnostic information on message detection and decoding performance.

V. Summary and Conclusion

In this paper, we introduced two new algorithms for modeling the effects of the underwater sound channel on the transmission

of a known time series. The VirTEX for platform motion algorithm can address situations where the source and/or the receiver exhibit steady motion. The VirTEX for sea-surface dynamics algorithm can address the effects of the moving air–sea interface. Both algorithms represent improvements in runtime performance compared to the more rigorous VirTEX algorithm, in exchange for less, but typically acceptable levels of accuracy.

In our example applications of these new algorithms, we clearly demonstrated that predicting the performance of acoustic modems goes beyond a simple knowledge of the transmission loss.

References

[1] C. Bjerrum-Niese, "Influence of the dynamic sea surface on underwater acoustic communication," Ph.D. dissertation, Dept. Manuf. Eng. Ind. Acoust., Tech. Univ. Denmark, Lyngby, Denmark, 1998.

[2] C. Bjerrum-Niese, R. Lützen, and L. Jensen, "Ray tracing in a turbulent, shallow-water channel," *J. Acoust. Soc. Amer.*, vol. 103, no. 5, pp. 2751–2751, 1998.

[3] E. Svensson, "Physical modelling of acoustic shallow-water communication channels," Ph.D. dissertation, Aeronaut. Veh. Eng. Dept., Royal Institute of Technology (KTH), Stockholm, Sweden, 2007.

[4] N. Goddard and M. Launder, "Standardised testing of acoustic communications modems using a high fidelity simulator," in *Proc. 3rd Underwater Acoust. Meas. Conf.*, Nafplion, Greece, 2009.

[5] S. Morgan, N. Goddard, S. Pointer, and P. Atkins, "High fidelity simulator for standardised testing of acoustic communications (AComms) modems and development of AComms systems for military applications," in *Proc. Undersea Defence Technol. Conf.*, Alicante, Spain, 2012.

[6] M. Siderius and M. B. Porter, "Modeling broadband ocean acoustic transmissions with time-varying sea surfaces," *J. Acoust. Soc. Amer.*, vol. 124, no. 1, pp. 137–150, 2008.

[7] C. Neipp, A. Hernández, J. J. Rodes, A. Márquez, T. Beléndez, and A. Beléndez, "An analysis of the classical Doppler effect," *Eur. J. Phys.*, vol. 24, no. 5, p. 497, 2003.

[8] Y.-S. Huang and K.-H. Lu, "Formulation of the classical and the relativistic Doppler effect by a systematic method," *Can. J. Phys.*, vol. 82, no. 11, pp. 957–964, 2004.

[9] L. R. Rabiner, R. W. Schafer, and C. M. Rader, "The chirp Z-transform algorithm," *IEEE Trans. Audio Electroacoust.*, vol. AU-17, no. 2, pp. 86–92, Jun. 1969.

[10] L. Wolff, E. Szczepanski, and S. B. Hoeher, "Acoustic underwater channel and network simulator," in *Proc. MTS/IEEE OCEANS Conf.*, Hampton Roads, VA, USA, 2012, DOI: 10.1109/OCEANS-Yeosu.2012.6263608.

[11] R. S. Kennedy, *Fading Dispersive Communication Channels*. New York, NY, USA: Wiley-Interscience, 1969, pp. 14–16.

[12] C. T. Tindle, G. B. Deane, and J. C. Preisig, "Reflection of underwater sound from surface waves," *J. Acoust. Soc. Amer.*, vol. 125, no. 1, pp. 66–72, 2009.

[13] D. B. Kilfoyle and A. B. Baggeroer, "The state of the art in underwater acoustic telemetry," *IEEE J. Ocean. Eng.*, vol. 25, no. 1, pp. 4–27, Jan. 2000.

[14] J. Proakis, *Digital Communications*, 4th ed. New York, NY, USA: McGraw-Hill, Aug. 2000, pp. 181–183.

John C. Peterson received the B.A. degree in mathematics and physics from Hamline University, St. Paul, MN, USA, in 1977, the M.S. degree in applied mathematics from the University of Illinois at Urbana–Champaign, Urbana, IL, USA, in 1979, and the M.S. degree in mechanical engineering science from the University of California at Berkeley, Berkeley, CA, USA, in 1984.

In 1979, he began working at the Lawrence Livermore National Laboratory, Livermore, CA, USA, as a Scientific Programmer. In 1985, he relocated to San Diego, CA, USA, where he has worked for Photon Research Associates, Science Applications International Corporation, AETC Inc., and the Orincon Corporation. Since 2006, he has worked as a Consultant in the area of scientific computing for various clients including Heat, Light, and Sound Research, Inc., La Jolla, CA, USA.

Michael B. Porter (M'95–SM'13) received the B.S. degree in applied mathematics from the California Institute of Technology (Caltech), Pasadena, CA, USA, in 1979 and the Ph.D. degree in applied mathematics and engineering sciences from Northwestern University, Evanston, IL, USA, in 1984.

In 1983, he began working at the Naval Ocean Systems Center, San Diego, CA, USA, and, in 1985, as a Research Physicist at the Naval Research Laboratory, Washington, DC, USA. In 1987, he became a Senior Scientist for NATO/SACLANT, La Spezia, Italy. He was also a Professor of Mathematics at the New Jersey Institute of Technology, Newark, NJ, USA, and an Assistant Vice President and Chief Scientist at Science Applications International Corporation, San Diego, CA, USA. He is currently the President and CEO of Heat, Light, and Sound Research, Inc., La Jolla, CA, USA.